J|A|C|S
ARTICLES
Published on Web 04/07/2006

X-Shaped Electro-optic Chromophore with Remarkably Blue-Shifted Optical Absorption. Synthesis, Characterization, Linear/Nonlinear Optical Properties, Self-Assembly, and Thin Film Microstructural Characteristics

Hu Kang,[†] Guennadi Evmenenko,[§] Pulak Dutta,[§] Koen Clays,[‡] Kai Song,[‡] and Tobin J. Marks*,[†]

Contribution from the Department of Chemistry and the Materials Research Center, and Department of Physics and Astronomy and the Materials Research Center, Northwestern University, 2145 Sheridan Road, Evanston, Illinois 60208-3113, and Department of Chemistry, University of Leuven, Celestijnenlaan 200D, B-3001 Leuven, Belgium

Received January 10, 2006; E-mail: t-marks@northwestern.edu

Abstract: A novel type of "X-shaped" two-dimensional electro-optic (EO) chromophore with extended conjugation has been synthesized and characterized. This chromophore is found to exhibit a remarkably blue-shifted optical maximum (357 nm in CH_2Cl_2) while maintaining a very large first hyperpolarizability (β). Hyper-Rayleigh Scattering (HRS) measurements at 800 nm provide a β_{zzz} value of 1840×10^{-30} esu. Self-assembled thin films of this chromophore were fabricated via a layer-by-layer chemisorptive siloxane-based approach. The chromophoric multilayers have been characterized by transmission optical spectroscopy, advancing contact angle measurements, synchrotron X-ray reflectivity, atomic force microscopy, and angle-dependent polarized second harmonic generation spectroscopy. The self-assembled chromophoric films exhibit a dramatically blue-shifted optical maximum (325 nm) while maintaining a large EO response ($\chi^{(2)}_{333} \sim 232$ pm/V at 1064 nm; $r_{33} \sim 45$ pm/V at 1310 nm). This work demonstrates an attractive approach to developing EO materials offering improved nonlinearity−transparency trade-offs.

Introduction

Realization of large-response molecule-based electro-optic (EO) materials and development of "all-organic" photonic devices are predicted to greatly enhance optical network speed, capacity, and bandwidth for high-speed optical communications, integrated optics, and optical data processing/storage. For these reasons, the quest for high-performance EO materials has been a very active research field.[1−3] Crucial synthetic challenges for large bulk EO response in these materials are that individual chromophore components have large molecular hyperpolarizabilities (β) and that they be arranged in a noncentrosymmetric architecture.[1−3] Among the various approaches to preparing suitable EO materials,[4−10] layer-by-layer chemisorptive siloxane-based self-assembly (SA) for templated formation of intrinsically polar arrays of high-β chromophores is particularly attractive in that it yields self-assembled superlattices (SASs) that can be grown on silicon or a variety of related substrates with dense

[†] Department of Chemistry, Northwestern University.
[§] Department of Physics and Astronomy, Northwestern University.
[‡] University of Leuven.

(1) (a) *Characterization Techniques and Tabulations for Organic Nonlinear Optical Materials*; Kuzyk, M. G., Dirk, C. W., Eds.; Marcel Dekker: New York, 1998. (b) *Nonlinear Optics of Organic Molecules and Polymers*; Nalwa, H. S., Miyata, S., Eds.; CRC Press: Boca Raton, FL, 1997. (c) Organic Nonlinear Optical Materials. In *Advances in Nonlinear Optics*; Bosshard, C., Sutter, K., Prêtre, P., Hulliger, J., Flörsheimer, M., Kaatz, P., Günter, P., Eds.; Gordon & Breach: Amsterdam, 1995; Vol. 1. (d) *Molecular Nonlinear Optics: Materials, Physics, Devices*; Zyss, J., Ed.; Academic Press: Boston, MA, 1994. (e) *Introduction to Nonlinear Optical Effects in Molecules and Polymers*; Prasad, P. N., Williams, D. J., Eds.; John Wiley: New York, 1991. (f) *Materials for Nonlinear Optics: Chemical Perspectives*; Marder, S. R., Stucky, G. D., Sohn, J. E., Eds.; ACS Symposium Series Vol. 455; American Chemical Society: Washington, DC, 1991.

(2) (a) Dalton, L. R. *Pure Appl. Chem.* **2004**, *76*, 1421. (b) Kajzar, F.; Lee, K.-S.; Jen, A. K.-Y. *Adv. Polym. Sci.* **2003**, *161*, 1. (c) Dalton, L. *Adv. Polym. Sci.* **2002**, *158*, 1. (d) Dalton, L. R.; Steier, W. H.; Robinson, B. H.; Zhang, C.; Ren, A.; Garner, S.; Chen, A.; Londergan, T.; Irwin, L.; Carlson, B.; Fifield, L.; Phelan, G.; Kincaid, C.; Amend, J.; Jen, A. *J. Mater. Chem.* **1999**, *9*, 1905. (e) *Molecular Nonlinear Optics: Materials, Phenomena and Devices*; Zyss, J., Ed.; *Chem. Phys.* **1999**, *245* (special issue). (f) Verbiest, T.; Houbrechts, S.; Kauranen, M.; Clays, K.; Persoons, A. *J. Mater. Chem.* **1997**, *7*, 2175. (g) Marks, T. J.; Ratner, M. A. *Angew. Chem., Int. Ed. Engl.* **1995**, *34*, 155.

(3) (a) Dalton, L. R.; Jen, A. K.-Y.; Steier, W. H.; Robinson, B. H.; Jang, S.-H.; Clot, O.; Song, H. C.; Kuo, Y.-H.; Zhang, C.; Rabiei, P.; Ahn, S.-W.; Oh, M. C. *SPIE Proc.* **2004**, *5351*, 1. (b) Lee, M.; Katz, H. E.; Erben, C.; Gill, D. M.; Gopalan, P.; Heber, J. D.; McGee, D. J. *Science* **2002**, *298*, 1401. (c) Ma, H.; Jen, A. K.-Y.; Dalton, L. R. *Adv. Mater.* **2002**, *14*, 1339. (d) Shi, Y.; Zhang, C.; Zhang, H.; Bechtel, J. H.; Dalton, L. R.; Robinson, B. H.; Steier, W. H. *Science* **2000**, *28*, 119.

(4) (a) van der Boom, M. E. *Angew. Chem., Int. Ed.* **2002**, *41*, 3363. (b) Ma, H.; Chen, B.; Sassa, T.; Dalton, L. R.; Jen, A. K.-Y. *J. Am. Chem. Soc.* **2001**, *123*, 986. (c) Hayden, L. M.; Kim, W.-K.; Chafin, A. P.; Lindsay, G. A. *Macromolecules* **2001**, *34*, 1493. (d) Jiang, H.; Kakkar, A. K. *J. Am. Chem. Soc.* **1999**, *121*, 3657. (e) Yitzchaik, S.; Di Bella, S.; Lundquist, P. M.; Wong, G. K.; Marks, T. J. *J. Am. Chem. Soc.* **1997**, *119*, 2995. (f) Ye, C.; Minami, N.; Marks, T. J.; Yang, J.; Wong, G. K. *Macromolecules* **1988**, *21*, 2899. (g) Ye, C.; Marks, T. J.; Yang, J.; Wong, G. K. *Macromolecules* **1987**, *20*, 2322.

(5) (a) Schwartz, H.; Mazor, R.; Khodorkovsky, V.; Shapiro, L.; Klug, J. T.; Kovalev, E.; Meshulam, G.; Berkovic, G.; Kotler, Z.; Efrima, S. *J. Phys. Chem. B* **2001**, *105*, 5914. (b) Ricceri, R.; Neto, C.; Abbotto, A.; Facchetti, A.; Pagani, G. A. *Langmuir* **1999**, *15*, 2149. (c) Roberts, M. J.; Lindsay, G. A.; Herman, W. N.; Wynne, K. J. *J. Am. Chem. Soc.* **1998**, *120*, 11202. (d) Wijekoon, W. M. K. P.; Wijayu, S. K.; Bhawalkar, J. D.; Prasad, P. N.; Penner, T. L.; Armstrong, N. J.; Ezenyilimba, M. C.; Williams, D. J. *J. Am. Chem. Soc.* **1996**, *118*, 4480. (e) Ashwell, G. J.; Jackson, P. D.; Crossland, W. A. *Nature* **1994**, *368*, 438.

 10.1021/ja060185v CCC: $33.50

Chart 1. High-β Chromophoric Building Blocks Used in Self-Assembled Superlattices

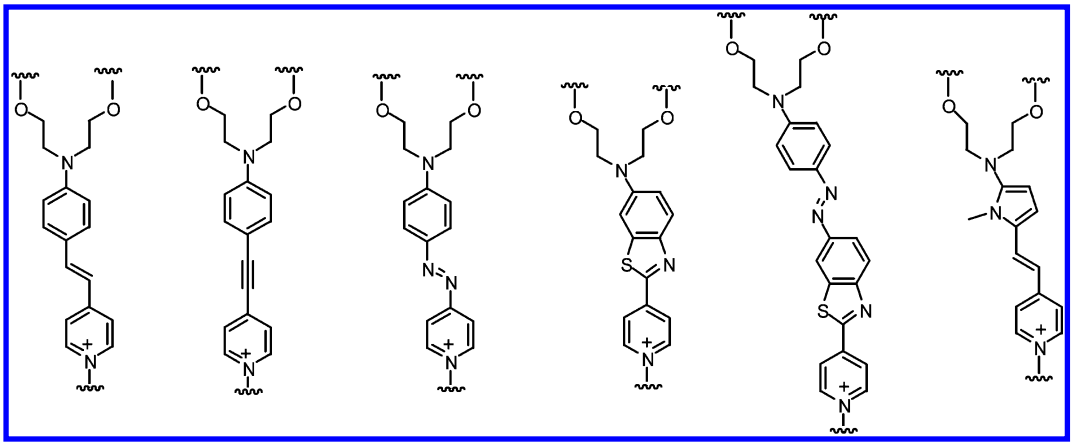

chromophore packing, covalently cross-linked microstructural orientation, high thermal stability, and large EO coefficients. These characteristics eliminate the need for postdeposition processes, such as electric field poling, allow ready device integration, and therefore significantly reduce device design complexity.[9,10] To date, the large-β chromophore building blocks incorporated into such SAS materials,[9,10] as well as those employed in typical poled polymer[4] and Langmuir−Blodgett-based films,[5] are devised according to common design motifs: conjugated one-dimensional (1D) planar conjugated π systems with end-capping electron donor and acceptor (D, A) substituents. Chromophores of this type usually exhibit a single intense low-lying longitudinal charge-transfer (CT) excitation and possess optical nonlinearities which are essentially 1D in nature, that is, dominated by a single β tensor component. Considerable, elegant efforts have striven to increase β by optimizing D/A strengths and/or the conjugation pathways of such 1D chromophores.[11] However, increases in β for such chromophores are almost invariably accompanied by bathochromic shifts of the optical maximum, eroding the optical transparency in the NIR region essential for many EO applications. Furthermore, molecules with extended π systems and low-lying excited states are frequently subject to chemical and thermal instability.[12] Alternative design strategies at the molecular level would therefore be desirable, especially for the siloxane-based SAS strategy building blocks where pyridinium and aminophenyl fragments are exclusively utilized as D/A functionalities/covalent linkers, and the key component to tune chromophore molecular properties is the engineering of the conjugative pathway.[9,10] Recent investigations have revealed that unconventional NLO chromophores with multiple donor−acceptor substituents, hence multiple intramolecular charge transfer, ranging from dipolar "X-shaped"[13] and "Λ-shaped"[14] to octopolar molecules,[15] can afford 2D β tensor character where off-diagonal components

(6) (a) Bakiamoh, S. B.; Blanchard, G. J. *Langmuir* **2001**, *17*, 3438. (b) Neff, G. A.; Helfrich, M. R.; Clifton, M. C.; Page, C. J. *Chem. Mater.* **2000**, *12*, 2363. (c) Flory, W. C.; Mehrens, S. M.; Blanchard, G. J. *J. Am. Chem. Soc.* **2000**, *122*, 7976. (d) Roberts, M. J.; Lindsay, G. A.; Herman, W. N.; Wynne, K. J. *J. Am. Chem. Soc.* **1998**, *120*, 11202. (e) Hanken, D. G.; Naujok, R. R.; Gray, J. M.; Corn, R. M. *Anal. Chem.* **1997**, *69*, 240. (f) Katz, H. E.; Wilson, W. L.; Scheller, G. *J. Am. Chem. Soc.* **1994**, *116*, 6636.

(7) (a) Van Cott, K. E.; Guzy, M.; Neyman, P.; Brands, C.; Heflin, J. R.; Gibson, H. W.; Davis, R. M. *Angew. Chem., Int. Ed.* **2002**, *17*, 3226. (b) Facchetti, A.; van der Boom, M. E.; Abbotto, A.; Beverina, L.; Marks, T. J.; Pagani, G. A. *Langmuir* **2001**, *17*, 5939. (c) Huang, W.; Helvenston, M.; Casson, J. L.; Wang, R.; Bardeau, J.-F.; Lee, Y.; Johal, M. S.; Swanson, B. I.; Robinson, J. M.; Li, D.-Q. *Langmuir* **1999**, *15*, 6510. (d) Li, D.-Q.; Swanson, B. I.; Robinson, J. M.; Hoffbauer, M. A. *J. Am. Chem. Soc.* **1993**, *115*, 6975.

(8) (a) Facchetti, A.; Annoni, E.; Beverina, L.; Morone, M.; Zhu, P.; Marks, T. J.; Pagani, G. A. *Nat. Mater.* **2004**, *3*, 910. (b) Zhu, P.; Kang, H.; Facchetti, A.; Evmenenko, G.; Dutta, P.; Marks, T. J. *J. Am. Chem. Soc.* **2003**, *125*, 11496.

(9) (a) Zhu, P.; Kang, H.; van der Boom, M. E.; Liu, Z.; Xu, G.; Ma, J.; Zhou, D.; Ho, S.-T.; Marks, T. J. *SPIE Sympos. Proc.* **2004**, *5621*, 105. (b) van der Boom, M. E.; Evmenenko, G.; Yu, C.; Dutta, P.; Marks, T. J. *Langmuir* **2003**, *19*, 10531. (c) Zhu, P.; van der Boom, M. E.; Kang, H.; Evmenenko, G.; Dutta, P.; Marks, T. J. *Chem. Mater.* **2002**, *14*, 4982. (d) van der Boom, M. E.; Evmenenko, G.; Dutta, P.; Marks, T. J. *Langmuir* **2002**, *18*, 3704. (e) van der Boom, M. E.; Richter, A. G.; Malinsky, J. E.; Dutta, P.; Marks, T. J. *Chem. Mater.* **2001**, *13*, 15.

(10) (a) Facchetti, A.; Abbotto, A.; Beverina, L.; van der Boom, M. E.; Dutta, P.; Evmenenko, G.; Pagani, G. A.; Marks, T. J. *Chem. Mater.* **2003**, *15*, 1064. (b) Facchetti, A.; Abbotto, A.; Beverina, L.; van der Boom, M. E.; Dutta, P.; Evmenenko, G.; Pagani, G. A.; Marks, T. J. *Chem. Mater.* **2002**, *14*, 4996. (c) Lin, W.; Lee, T.-L.; Lyman, P. F.; Lee, J.; Bedzyk, M. J.; Marks, T. J. *J. Am. Chem. Soc.* **1997**, *119*, 2205. (d) Lin, W.; Lin, W.; Wong, G. K.; Marks, T. J. *J. Am. Chem. Soc.* **1996**, *118*, 8034. (e) Yitzchaik, S.; Marks, T. J. *Acc. Chem. Res.* **1996**, *29*, 197. (f) Lin, W.; Yitzchaik, S.; Lin, W.; Malik, A.; Durbin, M. K.; Richter, A. G.; Wong, G. K.; Dutta, P.; Marks, T. J. *Angew. Chem., Int. Ed. Engl.* **1995**, *34*, 1497. (g) Li, D.-Q.; Ratner, M. A.; Marks, T. J. *J. Am. Chem. Soc.* **1990**, *112*, 7389.

(11) (a) Kang, H.; Facchetti, A.; Zhu, P.; Jiang, H.; Yang, Y.; Cariati, E.; Righetto, S.; Ugo, R.; Zuccaccia, C.; Macchioni, A.; Stern, C. L.; Liu, Z.; Ho, S.-T.; Marks, T. J. *Angew. Chem., Int. Ed.* **2005**, *44*, 7922. (b) Liao, Y.; Eichinger, B. E.; Firestone, K. A.; Haller, M.; Luo, J.; Kaminsky, W.; Benedict, J. B.; Reid, P. J.; Jen, A. K.-Y.; Dalton, L. R.; Robinson, B. H. *J. Am. Chem. Soc.* **2005**, *127*, 2758. (c) Andreu, R.; Blesa, M. J.; Carrasquer, L.; Garín, J.; Orduna, J.; Villacampa, B.; Alcalá, R.; Casado, J.; Delgado, M. C. R.; Navarrete, J. T. L.; Allain, M. *J. Am. Chem. Soc.* **2005**, *127*, 8835. (d) Staub, K.; Levina, G. A.; Barlow, S.; Kowalczyk, T. C.; Lackritz, H. S.; Barzoukas, M.; Fort, A.; Marder, S. R. *J. Mater. Chem.* **2003**, *13*, 825. (e) Abbotto, A.; Beverina, L.; Bradamante, S.; Facchetti, A.; Klein, C.; Pagani, G. A.; Redi-Abshiro, M.; Wortmann, R. *Chem.−Eur. J.* **2003**, *9*, 1991. (f) Barlow, S.; Marder, S. R. *Chem. Commun.* **2000**, 1555. (g) Jen, A. K.-Y.; Ma, H.; Wu, X.; Wu, J.; Liu, S.; Marder, S. R.; Dalton, L. R.; Shu, C.-F. *SPIE Proc.* **1999**, *3623*, 112. (h) Albert, I. D. L.; Marks, T. J.; Ratner, M. A. J. *Am. Chem. Soc.* **1997**, *119*, 6575.

(12) Galvan-Gonzalez, A.; Belfield, K. D.; Stegeman, G. I.; Canva, M.; Marder, S. R.; Staub, K.; Levina, G.; Twieg, R. J. *J. Appl. Phys.* **2003**, *94*, 756 and references therein.

(13) (a) Sullivan, P. A.; Bhattacharjee, S.; Eichinger, B. E.; Firestone, K.; Robinson, B. H.; Dalton, L. R. *SPIE Proc.* **2004**, *5351*, 253. (b) Wortmann, R.; Lebus-Henn, S.; Reis, H.; Papadopoulos, M. G. *THEOCHEM* **2003**, *633*, 217. (c) Qin, A.; Bai, F.; Ye, C. *THEOCHEM* **2003**, *631*, 79. (d) Qin, A.; Yang, Z.; Bai, F.; Ye, C. *J. Polym. Sci., Part A* **2003**, *41*, 2846. (e) Kang, H.; Li, S.; Wang, P.; Wu, W.; Ye, C. *Synth. Met.* **2001**, *121*, 1469. (f) Wang, P.; Zhu, P.; Wu, W.; Kang, H.; Ye, C. *Phys. Chem. Chem. Phys.* **1999**, *1*, 3519. (g) Nalwa, H. S.; Watanabe, T.; Miyata, S. *Adv. Mater.* **1995**, *7*, 754.

(14) (a) Yang, M.; Champagne, B. *J. Phys. Chem. A* **2003**, *107*, 3942. (b) Ostroverkhov, V.; Petschek, R. G.; Singer, K. D.; Twieg, R. J. *Chem. Phys. Lett.* **2001**, *340*, 109. (c) Van Elshocht, S.; Verbiest, T.; Kauranen, M.; Ma, L.; Cheng, H.; Musick, K.; Pu, L.; Persoons, A. *Chem. Phys. Lett.* **1999**, *309*, 315. (d) Wolff, J. J.; Längle, D.; Hillenbrand, D.; Wortmann, R.; Matschiner, R.; Glania, C.; Krämer, P. *Adv. Mater.* **1997**, *9*, 138. (e) Wortmann, R.; Glania, C.; Krämer, P.; Matschiner, R.; Wolff, J. J.; Kraft, S.; Treptow, B.; Barbu, E.; Längle, D.; Görlitz, G. *Chem.−Eur. J.* **1997**, *3*, 1765. (f) Moylan, C. R.; Ermer, S.; Lovejoy, S. M.; McComb, I.-H.; Leung, D. S.; Wortmann, R.; Krämer, P.; Twieg, R *J. Am. Chem. Soc.* **1996**, *118*, 12950. (g) Wong, M. S.; Nicoud, J.-F.; Runser, C.; Fort, A.; Barzoukas, M.; Marchal, E. *Chem. Phys. Lett.* **1996**, *253*, 141. (h) Wortmann, R.; Krämer, P.; Glania, C.; Lebus S.; Detzer, N. *Chem. Phys.* **1993**, *173*, 99.

Chart 2

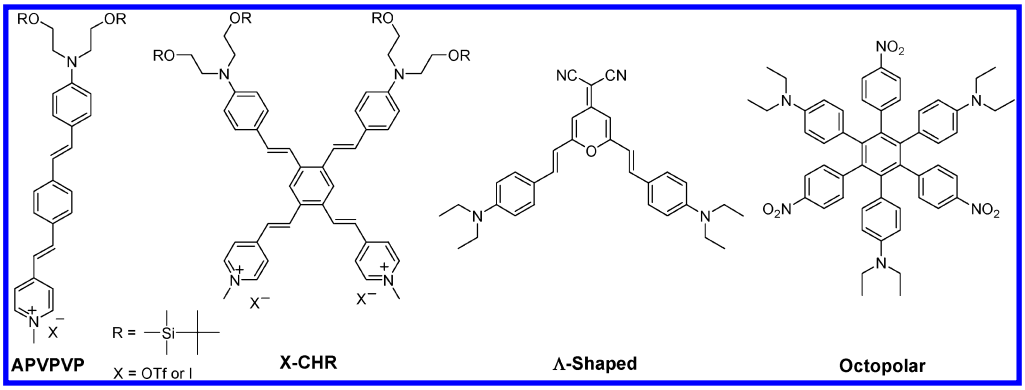

become significant, offering potential advantages over 1D chromophores, such as increased β responses without undesirable losses of transparency, and improved phase-matching via the larger off-diagonal components.[16] Moreover, off-diagonal contributions to the β tensor have been shown to significantly decrease NLO film anisotropy, opening new possibilities for the development of polarization-independent materials that would be suitable for optical telecommunications.[17] Regarding siloxane-based SAS fabrication strategies, dipolar X-shaped molecules which possess two D/A pairs straddling the C_{2v} symmetry axis (also the molecular dipolar axis; see structure below) might offer not only possible relaxation of nonlinearity−transparency trade-offs but also enhanced microstructural regularity and orientational stability via chelative, double chemisorptive anchoring at both donor and acceptor ends of the synthon. To date, however, no studies have reported implementing 2D EO chromophore building blocks in SAS strategies, and there have been only few experimental studies incorporating dipolar 2D chromophores in LB or poled polymer thin films.[13d,e,15a,b] In this contribution, we present a full discussion of the synthesis, characterization, and chemisorptive self-assembly into intrinsically acentric EO-active thin films of the novel type of X-shaped 2D chromophore, **X-CHR**, containing a central aromatic core fused to extended conjugated D/A aminophenyl/pyridinium groups. Here the optical transition dipoles are arranged to couple in such a manner as to drastically blue-shift λ_{max} while maintaining a very large β response. AM1/ZINDO computations predict $\beta_{\omega=0} = 407 \times 10^{-30}$ esu with a HOMO−LUMO CT excitation $\lambda_{max} = 369$ nm for this chromophore versus $\beta_{\omega=0} = 312 \times 10^{-30}$ esu with $\lambda_{max} = 551$ nm for the analogous 1D chromophore **APVPVP**.[18] Even considering a slightly lower value of the computed molecular mass normalized NLO response (β/M_w) of 0.56×10^{-30} esu for **X-CHR** versus 0.77×10^{-30} esu for its 1D analogue, **APVPVP**, this minor attenuation in hyperpolarizability still represents a small compromise considering the great enhancement of the optical transparency predicted. Some preliminary experimental results on this new π chromophore have been previously communicated.[19] We present in this contribution a detailed discussion of chromophore synthetic approaches, solution structural characterization, linear optical (UV−vis) and NLO (Hyper-Rayleigh Scattering) spectroscopic observations, and efficient self-assembly into siloxane-based superlattices of this new X chromophore. We report detailed characterization of these self-assembled chromophoric films using a combination of techniques, including transmission optical spectroscopy, advancing contact angle measurements, synchrotron X-ray reflectivity, atomic force microscopy, and angle-dependent polarized SHG spectroscopy. It will be seen that X-chromophore-derived SAS films exhibit a remarkably blue-shifted optical maximum while maintaining a very large EO response, as well as high structural regularity.

Experimental Section

Materials and Methods. All reagents were purchased from Aldrich Chemical Co. and used as received unless otherwise indicated. THF was distilled from sodium/benzophenone and methylene chloride from calcium hydride. Toluene and pentane were dried/deoxygenated by passing through two packed columns of activated alumina and Q5 under nitrogen pressure and were tested using benzophenone ketyl in ether solution. The reagent 4,5-dibromo-*o*-xylene was purchased from Alfa Aesar. The reagents 1,2-dibromo-4,5-bis(bromomethyl)benzene (**1**),[20] [(4,5-dibromo-1,2-phenylene)bis(methylene)]bisphosphonic acid tetraethyl ester (**2**),[21] and 4-*N*,*N*-bis(2-*tert*-butyldimethylsiloxyethyl)aminobenzaldehyde (**3**)[22] were synthesized according to the literature procedures. The coupling agent dichloroiodo-(4-iodomethylphenyl)-silane was prepared following procedures previously described.[9c,10a,b] Single-crystal silicon(111) substrates were purchased from Semiconductor Processing Company, Inc. NMR spectra were recorded on a Varian Mercury 400 MHz or Varian INOVA 500 MHz spectrometer. Mass spectra were recorded on a Micromass Quattro II Triple Quadrupole HPLC/MS/MS mass spectrometer. Elemental analyses were performed by Midwest Microlabs. UV−vis spectra were recorded on a Cary 1E or Cary 5000 spectrophotometer. Thermal analysis (TGA) was performed with a TA Instruments SDT 2960 simultaneous DTA-TGA instrument. Polarized second harmonic generation measurements were carried out in the transmission mode with a Q-switched Nd:YAG laser

(15) (a) Traber, B.; Wolff, J. J.; Rominger, F.; Oeser, T.; Gleiter, R.; Goebel, M.; Wortmann, R. *Chem.—Eur. J.* **2004**, *10*, 1227. (b) Wolff, J. J.; Segler, F.; Matschiner, R.; Wortmann, R. *Angew. Chem., Int. Ed.* **2000**, *39*, 1436. (c) Brasselet, S.; Cherioux, F.; Audebert, P.; Zyss, J. *Chem. Mater.* **1999**, *11*, 1915. (d) Lee, Y.-K.; Jeon, S.-J.; Cho, M. *J. Am. Chem. Soc.* **1998**, *120*, 10921. (e) Brasselet, S.; Zyss, J. *J. Opt. Soc. Am. B* **1998**, *15*, 257.
(16) (a) Miyata, S.; Sasabe, H. *Poled Polymers and Their Applications to SHG and EO Devices*; Gordon and Breach Science: Australia, 1997. (b) Yamamoto, H.; Katogi, S.; Watanabe, T.; Sato, H.; Miyata, S.; Hosomi, T. *Appl. Phys. Lett.* **1992**, *60*, 935. (c) Zyss, J.; Oudar, L. L. *Phys. Rev. A* **1982**, *26*, 2016.
(17) (a) Di Bella, S.; Fragalá, I.; Ledoux, I.; Zyss, J. *Chem.—Eur. J.* **2001**, *7*, 3738. (b) Donval, A.; Toussaere, E.; Hierle, R.; Zyss, J. *J. Appl. Phys.* **2000**, *87*, 3258.
(18) Keinan, S.; Ratner, M. A.; Marks, T. J. unpublished results.
(19) Kang, H.; Zhu, P.; Yang, Y.; Facchetti, A.; Marks, T. J. *J. Am. Chem. Soc.* **2004**, *126*, 15974.
(20) Rivera, J. M.; Martin, T.; Rebek, J., Jr. *J. Am. Chem. Soc.* **2001**, *123*, 5213.
(21) Kimura, M.; Narikawa, H.; Ohta, K.; Hanabusa, K.; Shirai, H.; Kobayashi, N. *Chem. Mater.* **2002**, *14*, 2711.
(22) Zhang, C.; Wang, C.; Dalton, L. R. *Macromolecules* **2001**, *34*, 253.

operating at 1064 nm, with a pulse width of 3 ns at a frequency of 10 Hz. The details of this setup can be found elsewhere.[23]

Synthesis of 1,2-Dibromo-4,5-bis{(*E*)-2-[*p*-*N*,*N*-bis(2-*tert*-butyldimethylsiloxyethyl)aminophenyl]ethenyl}benzene (4). To a yellow solution of **2** (8.04 g, 15.0 mmol) in dry THF (45 mL) was added sodium methoxide (8.68 g, 28% methanol solution, 45.0 mmol) dropwise at −15 to −20 °C, and the mixture was stirred at this temperature for an additional 1 h. Next, benzaldehyde **3** (14.67 g, 33.0 mmol) was slowly added to the reaction mixture at −15 to −20 °C over the course of 40 min and then stirred at this temperature for an additional 30 min. The reaction mixture was allowed to warm to room temperature, covered with aluminum foil, and stirred at room temperature for 10 h. To the resulting orange solution was added saturated aqueous NH_4Cl solution (45 mL) at 0−5 °C in an ice bath. The mixture was then extracted with diethyl ether (3 × 75 mL), and the ether layer was successively washed with water, saturated aqueous NH_4Cl, and brine, dried over $NaSO_4$, filtered, and concentrated in vacuo. The resulting orange oil was purified by flash chromatography on silica gel, eluting with 10:1 hexane:diethyl ether, to give 8.90 g (53.8%) of the title compound as a yellow sticky oil. ^{1}H NMR (400 MHz, CD_2Cl_2): δ 7.799 (s, 2H), 7.382 (d, J = 8.4 Hz, 4H), 7.096 (d, J = 16.0 Hz, 2H), 6.928 (d, J = 16.0 Hz, 2H), 6.695 (d, J = 8.4 Hz, 4H), 3.778 (t, J = 6.4 Hz, 8H), 3.547 (t, J = 6.4 Hz, 8H), 0.892 (s, 36H), 0.040 (s, 24H). ^{13}C NMR (100 MHz, CD_2Cl_2): δ 148.515, 137.415, 132.736, 130.818, 128.467, 124.911, 122.417, 119.323, 111.967, 60.900, 54.083, 26.294, 18.799, −4.916. MS (FAB): *m*/*z* 1103.2 [M^+, 100]. MS (high resolution, FAB): *m*/*z* 1100.4340 [M^+]; calcd, 1100.4344. Anal. Calcd for $C_{54}H_{90}Br_2N_2O_4Si_4$: C, 58.78; H, 8.22; N, 2.54. Found: C, 59.01; H, 8.09; N, 2.54.

Synthesis of 1,2-Bis((*E*)-2-pyridin-4-ylvinyl)-4,5-bis{(*E*)-2-[*p*-*N*,*N*-bis(2-*tert*-butyldimethylsiloxyethyl)aminophenyl]ethenyl}benzene (BPBAB). A flame-dried sealable Schlenk tube was charged with **4** (1.0 g, 0.90 mmol), $Pd(OAc)_2$ (20 mg, 0.090 mmol), and PPh_3 (23.6 mg, 0.090 mmol), evacuated, and then backfilled with N_2. Next, 4-vinylpyridine (0.96 g, 9.0 mmol) and dry Et_3N (1 mL) were added under a N_2 flow. The Schlenk tube was then sealed, and the mixture was degassed by three freeze−thaw cycles and backfilled with N_2. The mixture was then covered with aluminum foil and stirred at 100 °C for 3 days. The resulting yellow solid was next dissolved in CH_2Cl_2 (50 mL) and washed with water. The organic layer was separated, dried over $MgSO_4$, filtered, and concentrated in vacuo to give a yellow solid. The crude product was recrystallized from acetone to give 0.70 g (67%) of the title compound as a yellow solid. Mp 199−200 °C. ^{1}H NMR (400 MHz, CD_2Cl_2): δ 8.585 (d, J = 5.6 Hz, 4H), 7.843 (s, 2H), 7.705 (d, J = 16.8 Hz, 2H), 7.442 (d, J = 8.8 Hz, 4H), 7.423 (d, J = 5.6 Hz, 4H), 7.284 (d, J = 16.0 Hz, 2H), 7.076 (d, J = 16.0 Hz, 2H), 7.052 (d, J = 16.0 Hz, 2H), 7.736 (d, J = 8.4 Hz, 4H), 3.814 (t, J = 6.4 Hz, 8H), 3.583 (t, J = 6.4 Hz, 8H), 0.922 (s, 36H), 0.073 (s, 24H). ^{13}C NMR (100 MHz, CD_2Cl_2): δ 150.758, 148.520, 144.990, 137.228, 134.125, 132.033, 130.704, 128.803, 128.502, 125.472, 124.681, 121.351, 121.041, 112.124, 60.952, 54.118, 26.285, 18.742, −4.979. MS (FAB): *m*/*z* 1151.5 [M^+, 100]. MS (high resolution, FAB): *m*/*z* 1150.6976 [M^+]; calcd, 1150.6978. Anal. Calcd for $C_{68}H_{102}N_4O_4Si_4$: C, 70.90; H, 8.93; N, 4.86. Found: C, 70.82; H, 8.75; N, 4.84.

Synthesis of Methylpyridinium X Chromophore (X-CHR). A flame-dried Schlenk flask was charged with **BPBAB** (115 mg, 0.10 mmol) and then evacuated and backfilled with N_2. Next, dry methylene chloride (5 mL) was added via syringe under N_2, and the solution was stirred at 0 °C. Methyl triflate (32.8 mg, 22.6 μL, 0.20 mmol) was next added dropwise via syringe under N_2. The resulting mixture was stirred at room temperature for 10 min. The solvent was then evaporated in vacuo to give 147 mg (100%) of analytically pure product as a dark solid. ^{1}H NMR (400 MHz, CD_2Cl_2): δ 8.293 (d, J = 4.8 Hz, 4H), 8.258 (d, J = 5.6 Hz, 4H), 7.817 (d, J = 16.0 Hz, 2H), 7.707 (s, 2H), 7.453 (d, J = 8.0 Hz, 4H), 7.181 (d, J = 16.0 Hz, 2H), 7.120 (d, J = 16.0 Hz, 2H), 6.876 (d, J = 16.0 Hz, 2H), 6.744 (d, J = 8.0 Hz, 4H), 3.839 (s, 6H), 3.821 (s, 8H), 3.613 (s, 8H), 0.921 (s, 36H), 0.083 (s, 24H). ^{13}C NMR (100 MHz, CD_2Cl_2): δ 153.570, 148.766, 144.553, 138.438, 137.037, 132.706, 129.239, 125.745, 125.036, 124.672, 124.371, 119.886, 119.676, 112.033, 61.006, 54.173, 47.640, 26.266, 18.732, −4.970. MS (ESI): *m*/*z* 1329.9 [$M^+ - TfO^-$, 100], 590.9 [$M^{2+} - 2TfO^-$, 45]. Anal. Calcd for $C_{72}H_{108}F_6N_4O_{10}S_2Si_4 \cdot 2H_2O$: C, 57.04; H, 7.45; N, 3.70. Found: C, 56.81; H, 7.29; N, 3.68.

Hyper-Rayleigh Scattering (HRS) Measurements. General details of the hyper-Rayleigh scattering (HRS) experiment have been discussed elsewhere,[24] and the experimental procedure and data analysis protocol used were also previously described.[25] All measurements were performed using the 800 nm fundamental of a regenerative mode-locked Ti^{3+}:sapphire laser (Spectra Physics, model Tsunami, 100 fs pulses, 1 W, 80 MHz). Measurements were carried out in methanol, with crystal violet chloride (CV) as an external reference ($\beta_{xxx} = 338 \times 10^{-30}$ esu in methanol at 800 nm), taking into account the difference in symmetry (octopolar for CV and dipolar for the X chromophore). The sample was dissolved in methanol and passed through 0.2 μm filters. Dilute solutions (10^{-5}−10^{-6} M) were used to ensure a linear dependence of $I_{2\omega}/I_\omega^2$ on solute concentration, precluding the need for Lambert−Beer correction for self-absorption of the second harmonic generation (SHG) signal. High-frequency femtosecond hyper-Rayleigh scattering (up to 240 MHz) was used to assess any multiphoton fluorescence contribution at 400 nm. No fluorescence effects were observed at 400 nm for **X-CHR**. A relative uncertainty of ±4.3% is estimated for the β value determined in the present experiments. The HRS depolarization ratio[26] was determined at 800 nm in methanol according to methodology reported previously.[27]

Self-Assembled Film Fabrication. Sodium lime glass, fused quartz, and silicon wafer substrates were cleaned by immersion in "piranha" solution (concentrated H_2SO_4:30% H_2O_2 7:3 v/v) at 80 °C for 1 h. After cooling to room temperature, they were rinsed repeatedly with deionized (DI) water and then subjected to an RCA-type cleaning protocol (H_2O:NH_4OH:30% H_2O_2 = 5:1:1 v/v/v, sonicated at room temperature for 40 min). The substrates were then washed with DI water and dried in an oven at 125 °C immediately before coupling agent deposition. Films were then fabricated via the iterative three-layer process:

(i) Self-Assembly of 4-$ICH_2C_6H_4SiCl_2I$. Freshly cleaned glass or silicon single-crystal substrates were immersed in a 15 mM solution of the coupling agent dichloroiodo-(4-iodomethylphenyl)silane in pentane under rigorously anhydrous and anaerobic conditions for 30 min at room temperature, washed copiously with dry pentane, sonicated in acetone for 1 min, and then dried under vacuum. A benzyl halide-functionalized surface is thereby obtained via the self-limiting chemisorption of the silane reagent.

(ii) Self-Assembly of the X Chromophore. The silylated substrates (after step i treatment) were spin-coated on both sides at 2500 rpm with a 5 mM solution of **BPBAB** in toluene inside a class 100 clean hood (Envirco) and then cured at 120 °C in a vacuum oven (0.4 Torr) for 40 min. After cooling to room temperature, the samples were washed with toluene and acetone to remove any residual **BPBAB** and dried under vacuum.

(iii) Self-Assembly of Octachlorotrisiloxane. The glass or silicon single-crystal substrates after the steps i and ii treatments were then

(23) Yitzchaik, S.; Roscoe, S. B.; Kakkar, A. K.; Allan, D. S.; Marks, T. J.; Xu, Z.; Zhang, T.; Lin, W.; Wong, G. K. *J. Phys. Chem.* **1993**, *97*, 6958.

(24) (a) Terhune, R. W.; Maker, P. D.; Savage, C. M. *Phys. Rev. Lett.* **1965**, *14*, 681. (b) Clays, K.; Persoons, A. *Phys. Rev. Lett.* **1991**, *66*, 2980. (c) Clays, K.; Persoons, A. *Rev. Sci. Instrum.* **1992**, *63*, 3285. (d) Hendrickx, E.; Clays, K.; Persoons, A. *Acc. Chem. Rev.* **1998**, *31*, 675.

(25) (a) Clays, K.; Olbrechts, G.; Munters, T.; Persoons, A.; Kim, O.-K.; Choi, L.-S. *Chem. Phys. Lett.* **1998**, *293*, 337. (b) Olbrechts, G.; Strobbe, R.; Clays, K.; Persoons, A. *Rev. Sci. Instrum.* **1998**, *69*, 2233.

(26) Heesink, G. J. T.; Ruiter, A. G. T.; van Hulst, N. F.; Bölger, B. *Phys. Rev. Lett.* **1993**, *71*, 999.

(27) Boutton, C.; Clays, K.; Persoons, A.; Wada, T.; Sasabe, H. *Chem. Phys. Lett.* **1998**, *286*, 101.

immersed in a 1:150 (v/v) solution of $Si_3O_2Cl_8$ in dry pentane for 30 min at room temperature under rigorously anhydrous and anaerobic conditions, then removed, washed with copious amounts of dry pentane and methanol, and sonicated in acetone for 1 min.

Specular X-ray Reflectivity (XRR). XRR studies were performed at beamline X23B of the National Synchrotron Light Source using a Huber four-circle diffractometer in the specular reflection mode (i.e., the incident angle is equal to the exit angle). X-rays of energy $E = 10$ keV ($\lambda = 1.24$ Å) were used for all measurements. The beam size was 0.4 mm vertically and 1.5 mm horizontally. The samples were placed under helium during the measurements to reduce the background scattering from the ambient gas and radiation damage. The experiments were performed at room temperature. The off-specular background was measured and subtracted from the specular counts. Details of the data acquisition and analysis procedures are given elsewhere.[28]

Results

The synthesis of the X chromophore via a straightforward multi-step route is first reported. The new compounds are fully characterized via conventional analytical/spectroscopic techniques. In addition, thermal stability is quantified by thermogravimetric (TGA). The chromophore linear optical response properties in solution are studied by optical absorption spectroscopy (UV−vis). It will be seen that this chromophore indeed exhibits a remarkable blue-shifted λ_{max}. The X chromophore solution structure is next defined by concentration-dependent optical and NMR spectroscopies. Hyper-Rayleigh Scattering (HRS) measurements reveal a very large HRS-derived β_{zzz} value. We further demonstrate that this new chromophore can be incorporated into self-assembled thin films via a three-step layer-by-layer self-assembly technique.[10] The resulting thin films are characterized by optical transmission spectroscopy (to characterize the fidelity of the assembly chemistry and the microstructural regularity), synchrotron X-ray reflectivity (XRR; to characterize film thickness, density, microstructural regularity, and interfacial roughness), advancing contact angle measurements (CA; to characterize surface energy), atomic force microscopy (AFM; to characterize surface morphology and roughness), and angle-dependent polarized SHG spectroscopy (to characterize NLO/EO response, microstructure, and polar regularity).

X Chromophore Synthesis and Characterization. The synthetic route to the X chromophore is summarized in Scheme 1. The phosphonate core **2** was obtained from 1,2-dibromo-4,5-bis(bromomethyl)benzene **1** via a Michaelis−Arbuzov reaction. The double Wittig−Horner reactions between 1 molar equiv of **2** and 2 equiv of TBDMS-protected 4-[*N*,*N*-bis(2-hydroxyethyl)amino]benzaldehyde **3** afford intermediate **4** in 54% yield. Subsequently, the double Heck coupling between **4** and excess 4-vinylpyridine (10 molar equiv) affords X chromophore precursor **BPBAB** in 67% yield. The dicationic methylpyridinium X chromophore (**X-CHR**) was next obtained quantitatively via MeOTf alkylation of **BPBAB**. All new compounds were fully characterized by conventional analytical/spectroscopic techniques, such as ^{1}H and ^{13}C NMR spectroscopy, mass spectrometry, and elemental analysis. Signals from **BPBAB** aromatic and vinyl protons in the aromatic region are difficult to assign due to overlapping of the vinyl and phenyl protons. Therefore ^{1}H 2D COSY NMR spectroscopy was used to help confirm the molecular connectivity (Figure 1). Thermal analysis (TGA) data (Figure 2) show that both **BPBAB** and **X-CHR** have high thermal stability ($T_d \approx 340$ °C for **BPBAB** and $T_d \approx 280$ °C for **X-CHR**).

Scheme 1. Synthetic Route to the X Chromophore **X-CHR**[a]

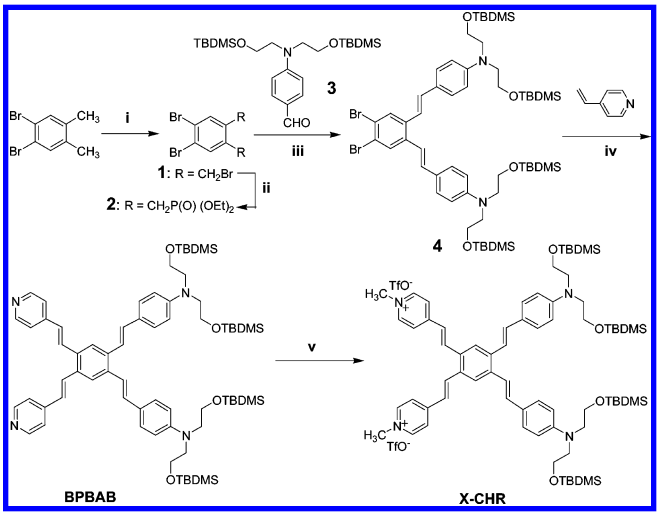

[a] Conditions: (i) NBS, CCl_4; (ii) $P(OEt)_3$; (iii) MeONa, THF; (iv) $Pd(OAc)_2/PPh_3$, Et_3N; (v) MeOTf, CH_2Cl_2.

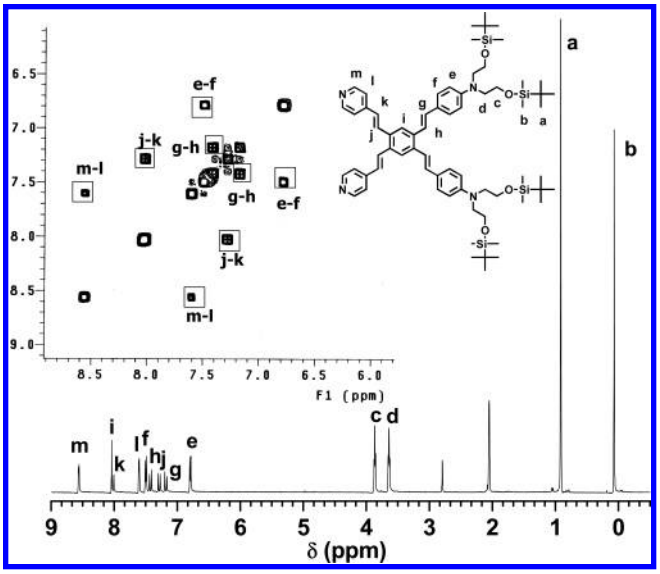

Figure 1. One-dimensional ^{1}H NMR spectrum (500 MHz, 25 °C) and ^{1}H 2D COSY NMR spectrum (500 MHz, 25 °C; inset) of X chromophore precursor (**BPBAB**) in acetone-d_6. Signals are assigned as indicated in the labeling scheme.

X Chromophore Solution Structure. Optical Spectroscopy. The **X-CHR** optical spectrum (Figure 3A) in CH_2Cl_2 solution consists of an intense band centered at 357 nm ($\epsilon = 120\,000$ L mol^{-1} cm^{-1}) involving $\pi \rightarrow \pi^*$ CT and a less intense, broad shoulder band at longer wavelength, ascribed to aggregation as supported by concentration-dependent optical absorption spectra (Figure 3B). Here significant spectral changes are observed upon varying the concentration over the range of 5×10^{-7} to 3×10^{-8} M, revealing an increase of the 357 nm CT band and concomitant diminution of the long-λ band upon dilution. A well-defined isosbestic point is observed in the concentration-dependent spectra and clearly indicates the presence of aggregation equilibria.[29] The bathochromic shifted aggregation band indicates that *J*-type aggregation occurs. This strong aggregation tendency is reasonable considering the large dipole

(28) Evmenenko, G.; van der Boom, M. E.; Kmetko, J.; Dugan, S. W.; Marks, T. J.; Dutta, P. *J. Chem. Phys.* **2001**, *115*, 6722.

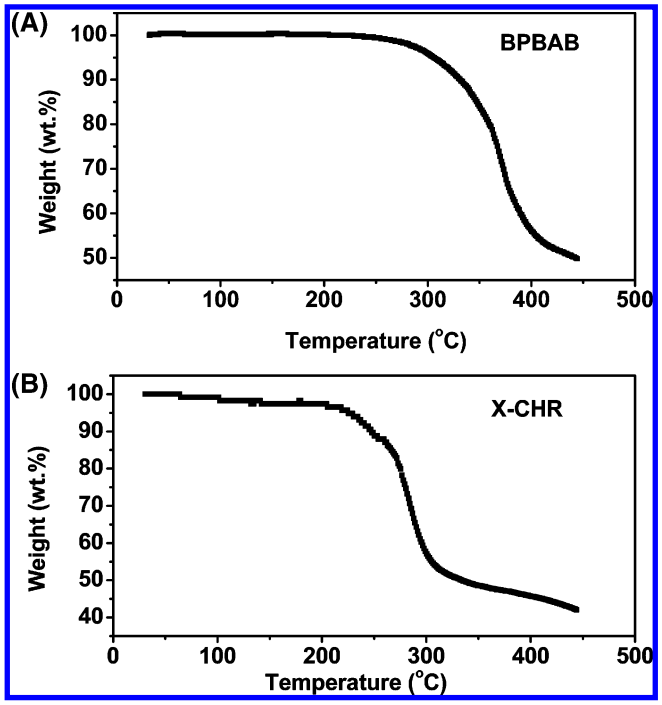

Figure 2. Thermogravimetric analysis (TGA) plots of weight percent versus temperature for chromophore precursor **BPBAB** (A) and chromophore **X-CHR** (B) under 1.0 atm N_2. The temperature ramp rate was 1.5 °C/min.

moment of **X-CHR** (the AM1-computed ground state dipole moment is 57.4 D).[18]

X Chromophore Solution Structure. Concentration-Dependent NMR Spectroscopy. The strong tendency for **X-CHR** aggregation in solution is also observed in concentration-dependent NMR experiments carried out in CD_2Cl_2 solution (Figure 4). The signals from *N*-methyl protons (H^n), outer pyridinium rings (H^m and H^l), central arene ring (H^i), and vinylene fragments (H^k, H^j, H^g, and H^h) are displaced significantly upfield in concentrated CD_2Cl_2 solution due to aggregation.[30] In contrast, the resonances of the protons on the outer phenylene rings (H^e and H^f) and ethanolamine groups (H^c and H^d) undergo negligible shifts with concentration. A similar phenomenon has also been reported for several 2D-conjugated poly(*p*-phenylenevinylene)-based molecules.[31] The present results can be explained if the planar conformation for the central part and two pyridine vinyl arms results in close stacking in solution through $\pi-\pi$ interactions, while the other two phenylenevinyl arms cannot undergo close stacking due to the bulky TBDMS protecting groups.

Hyper-Rayleigh Scattering Spectroscopy of the X Chromophore. The β_{zzz} component of the hyperpolarizability tensor for this chromophore has been determined at the molecular level by the femtosecond HRS techniques[24,25] using a 800 nm Ti^{3+}:sapphire laser. With the femtosecond pulses, it is possible to distinguish in the time domain between the immediate nonlinear scattering and the nanosecond time-delayed multiphoton fluorescence that, if present, results in overestimation of the hyperpolarizability magnitude.[25b] The experimental setup measures in the frequency domain, the apparent first hyperpolarizability as a function of amplitude modulation frequency. For higher frequencies, any multiphoton fluorescence contribution is diminished in amplitude and acquires a phase delay with respect to the scattering. The high-frequency limit of the apparent hyperpolarizability is therefore the accurate, fluorescence-free value. High-frequency femtosecond hyper-Rayleigh scattering measurements (up to 240 MHz) were carried out to assess any fluorescence contributions at 400 nm in **X-CHR**. The apparent dynamic hyperpolarizability as a function of modulation frequency does not exhibit any appreciable frequency dependence (with a slope of $(0.04 \pm 0.5) \times 10^{-30}$esu/MHz) or phase accumulation for increasing modulation frequencies, indicating that there are no fluorescence effects and that the signal is pure scattering. Therefore, the average value or the intercept of the hyperpolarizability magnitudes as a function of frequency, $(1840 \pm 80) \times 10^{-30}$ esu, was obtained for the β_{zzz} of **X-CHR**, assuming C_{2v} dipolar symmetry with a single major hyperpolarizability tensor element. This assumption can be verified by performing depolarization measurements,[26,27] where the depolarization ratio, that is, the ratio of HRS intensity in polarization paralleling the fundamental laser beam to that of the HRS in perpendicular polarization, is a sensitive function of molecular symmetry. The depolarization ratio of 5 is the

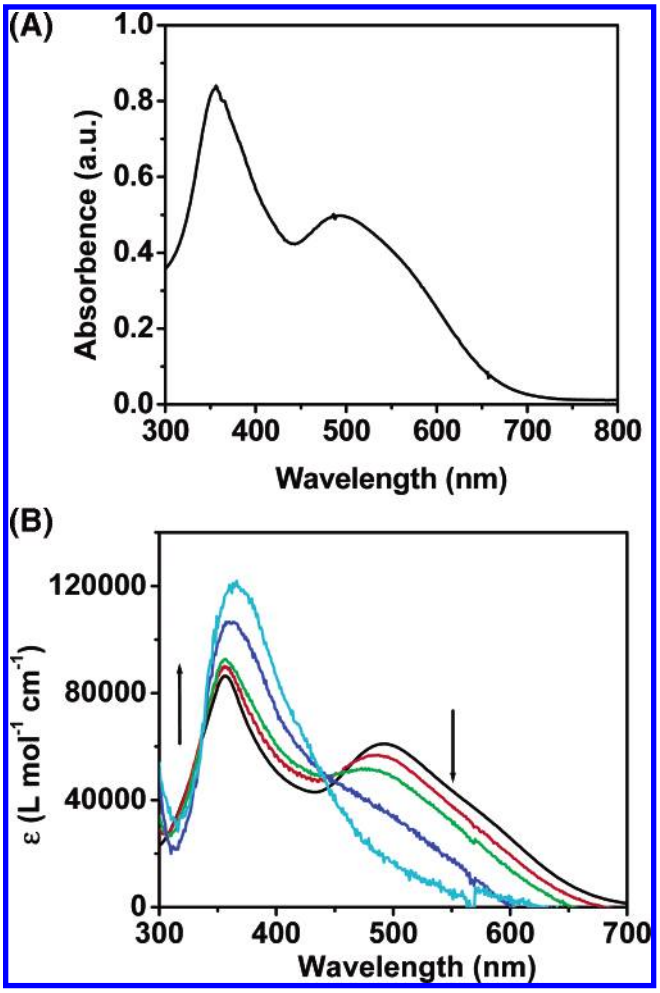

Figure 3. (A) Optical absorption spectrum of chromophore **X-CHR** in CH_2Cl_2 solution. (B) Concentration-dependent optical absorption spectra of chromophore **X-CHR** in CH_2Cl_2 solution. The arrows indicate changes of the monomer and the aggregation bands upon decreasing the concentration from 5×10^{-7} to 3×10^{-8} M.

(29) Dipolar molecule aggregation in solution is most frequently studied by optical spectrospy: Würthner, F.; Yao, S.; Debaerdemaeker, T.; Wortmann, R. *J. Am. Chem. Soc.* **2002**, *124*, 9431.
(30) Kraft, A. *Liebigs Ann/Recl.* **1997**, 1463.
(31) Niazimbetova, Z. I.; Christian, H. Y.; Bhandari, Y. J.; Beyer, F. L.; Galvin, M. E. *J. Phys. Chem. B* **2004**, *108*, 8673.

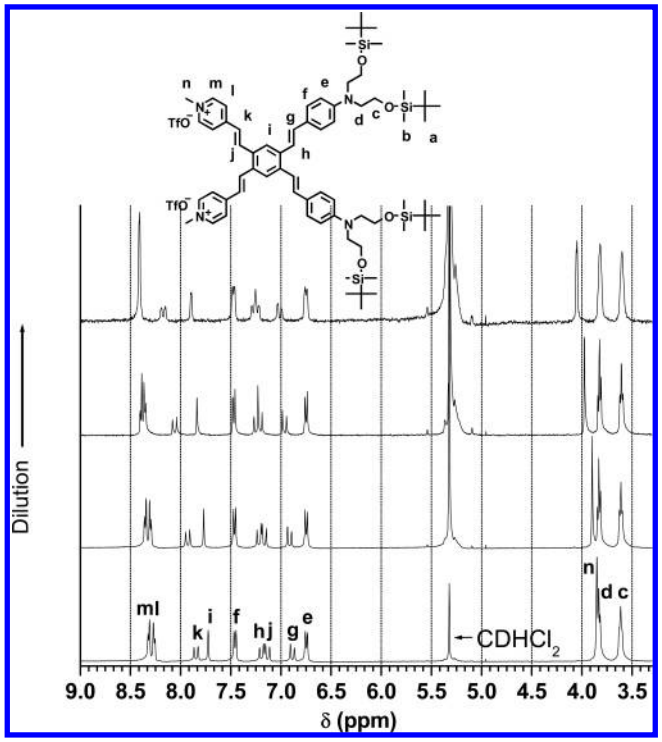

Figure 4. ^{1}H NMR spectra (400 MHz, 25 °C) of **X-CHR** in CD_2Cl_2 as a function of concentration. Signals are assigned as indicated in the labeling scheme. The unshifted high-field signals from the TBDMS protecting group protons are not shown here.

upper limit for a purely dipolar symmetry, that is, a single contributing tensor element in the limit of ideal experimental conditions, while the ratio if 1.5 is the lower limit for completely octopolar molecules. The HRS depolarization ratio determined here for **X-CHR** is 3.12 ± 0.06, consistent with a largely dipolar molecule. This value for the depolarization ratio corresponds to a ratio for diagonal β_{zzz} to off-diagonal β_{xzz} tensor element of -0.22. In comparison, the HRS depolarization ratio for Disperse Red 1 (DR1) under identical conditions is found to be 3.4 ± 0.2. The smaller estimated uncertainty for **X-CHR** with respect to DR1 is an indication of the more intense signal and greater signal-to-noise ratio. Note that the X chromophore is stable under the present HRS measurement conditions, as verified by UV−vis spectroscopy before and after the measurements, indicating excellent photochemical stability.

X Chromophore Self-Assembled Thin Film Fabrication. Layer-by-layer self-assembled X-chromophore-derived thin films were fabricated on a variety of substrates (glass, quartz, silicon) via an iterative three-step process (Scheme 2): (i) self-limited chemisorption of coupling agent 4-$ICH_2C_6H_4SiCl_2I$ onto the hydrophilic substrate surface; (ii) self-assembly of chromophore precursor **BPBAB** onto the benzyl halide-functionalized substrate via N-quaternization; and (iii) $Cl_3SiOSi(Cl_2)$-$OSiCl_3$ capping to planarize/cross-link/stabilize the polar structure into a 3D polysiloxane network and to simultaneously regenerate an active surface for subsequent layer deposition.

In step i, the freshly cleaned substrates were treated with a 15 mM solution of 4-$ICH_2C_6H_4SiCl_2I$ in dry pentane at room temperature for 30 min under rigorously anhydrous/anaerobic conditions, followed by washing with copious amounts of pentane and acetone to remove physisorbed coupling agent. Previous studies have established that this treatment (step i, Scheme 2) affords densely packed, self-assembled monolayers of benzyl iodide coupling agent on the surface.[10a,b] The self-assembled coupling layer was characterized by advancing aqueous contact angle (θ_a) measurements. The contact angle changes from 16° for SiO_2 to 68° for the silylated surface. This hydrophobic change in θ_a is consistent with the presence of benzyl iodide functionalities on the surface.[10a,b]

In step ii, the deposition of the X chromophore layers was achieved in a "topotactic" fashion.[10a−f] The substrates terminated with the benzyl iodide coupling layer were spin-coated with a thin layer of chromophore precursor **BPBAB**, followed by vacuum oven treatment at 120 °C/0.4 Torr. The chromophore deposition kinetics were monitored by SHG spectroscopy to optimize reaction conditions. Figure 5 shows the deposition kinetics at 120 °C/0.4 Torr. The 532 nm SHG output intensity ($I^{2\omega}$) reaches maximum at ~40 min and decreases at longer reaction times. The reason for the decline in $I^{2\omega}$ at longer reaction times may be the result of evolution in

Scheme 2. Self-Assembly of the X Chromophore to Prepare Polar Multilayers

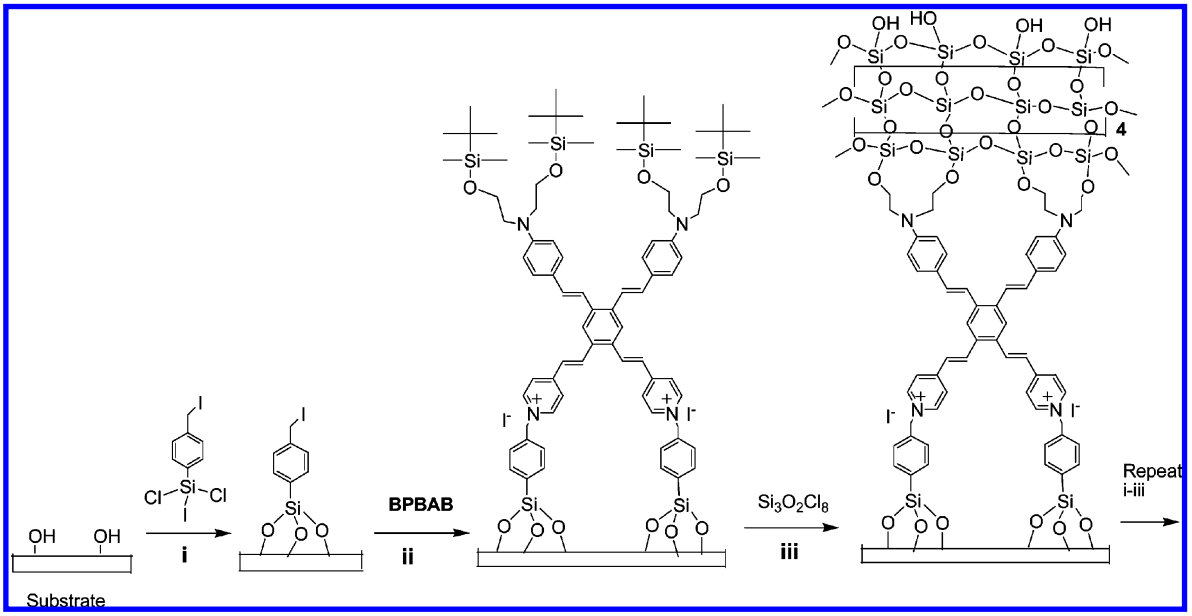

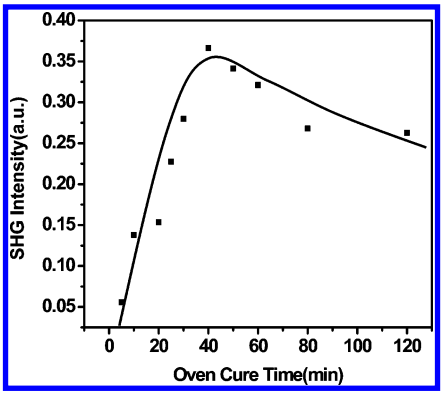

Figure 5. Second harmonic generation (SHG) response measurements as a function of reaction/deposition time for optimizing self-assembled X chromophore monolayer formation by vacuum oven treatment (step ii, Scheme 2) at 120 °C/0.4 Torr on a float glass substrate.

the chromophore tilt angle or slow structural reorganization of the uncapped monolayer. Variation in chromophore tilt angle as a function of coverage during monolayer formation has been observed in related self-assembling systems.[9c,10e] The samples were then washed with methanol and acetone to ensure the complete removal of excess **BPBAB** from the surface. Aqueous CA measurements on the chromophore-functionalized substrates (step ii, Scheme 2) reveal distinctly hydrophobic surfaces ($\theta_a \sim 76°$) in accordance with the formation of densely packed organic hydrocarbon films, exposing only the trialkylsilyl protecting groups at the outer surface.[9c]

The final (capping) step of the deposition sequence (step iii in Scheme 2) involves treatment of the chromophoric bilayers with octachlorotrisiloxane. Previous studies established that the reaction of octachlorotrisiloxane in dry pentane with trialkylsilyl-terminated chromophore layer surfaces and traces of adsorbed H_2O effects in situ chromophore deprotection and simultaneous formation of a hydrophilic polysiloxane surface.[9a−d] This capping step provides lateral structural stabilization/planarization via interchromophore cross-linking and also regenerates hydroxyl groups for the subsequent iterative superlattice assembly process.[9,10] The deposition of capping layers yields the expected hydrophilic change in θ_a; the advancing aqueous contact angle of the surface decreases from 76 to 18° after capping layer chemisorption.[9,10] This result is consistent with the regeneration of surface hydroxyl groups as a result of the capping layer deposition.

Film Microstructural/Electro-Optic Characterization. The resulting self-assembled multilayers were characterized by optical spectroscopy (UV−vis), synchrotron X-ray specular reflectivity (XRR), angle-dependent polarized second harmonic generation (SHG), and atomic force microscopy (AFM). The new films strongly adhere to the hydrophilic substrates and cannot be removed by the "Scotch tape decohesion test"[32] and are insoluble in common organic solvents. These films exhibit λ_{max} at the remarkably short wavelength of 325 nm (Figure 6). The linear dependence of the 325 nm absorbance on the number of layers (Figure 6 inset) indicates that essentially equal quantities of equivalently oriented chromophore molecules are deposited in each layer-forming step.

Specular X-ray reflectivity was used to probe microstructural evolution of these siloxane-based superlattices. Data for a series of 1−5 trilayers were obtained by fitting the multilayer reflectivity data to a Gaussian-step model.[28,33] In general, X-ray

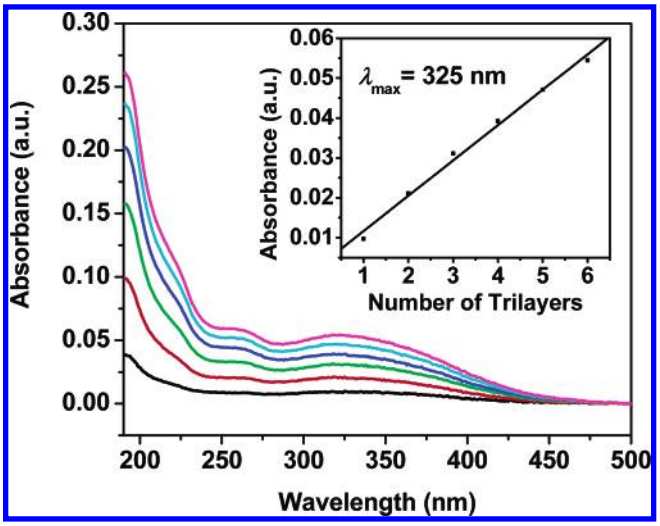

Figure 6. Optical absorption spectra of self-assembled X chromophore films grown on fused quartz as a function of the number of self-assembled layers. Inset: optical absorbance of the self-assembled films at $\lambda_{max} = 325$ nm as a function of the number of trilayers.

specular reflectivity is a function of the electron density profile $\rho(z)$ perpendicular to the sample surface. For the present systems, a model consisting of a silicon substrate and layers of different electron densities, ρ_i, with Gaussian broadened interfaces, σ_i, was used (eq 1).[28,33c]

$$\frac{R(q_z)}{R_F(q_z)} = \left| \sum_{i=0}^{N} \frac{(\rho_i - \rho_{i+1})}{\rho_0} e^{-iq_z D_i} e^{-q_z^2 \sigma_{i+1}^2/2} \right|^2 \qquad (1)$$

Here the wave vector transfer $|\boldsymbol{q}| = q_z = (4\pi/\lambda) \sin\theta$ is along the surface normal; ρ_0 is the electron density of the substrate ($=\rho_{Si}$), $\rho(z)$ is the electron density distribution inside the film averaged over the in-plane coherence length of the X-rays (usually $\sim 1-3\ \mu$m); $R_F(q_z)$ is the theoretical Fresnel reflectivity for an ideally flat substrate surface; N is the number of layers; $D_i = \sum_{j=1}^{i} T_j$ is the distance from the substrate surface to the ith interface, and T_i is the thickness of the ith layer. The reflectivity data were fit to such a model, the fitting parameters being the thickness and the electron density of each layer, and the root-mean-square width of each interface (the film-air interface corresponds to the film roughness). Note that eq 1 is valid for q_z larger than approximately twice the critical wave vector for total external reflection ($q_c = 0.0316$ Å^{-1} for Si), where refraction effects are negligible. Thus, the fits were performed using only data for which $q_z > 2q_c$. Figure 7A shows normalized reflectivity data (R/R_F) from a typical scan on a chromophore monolayer film (step ii, Scheme 2) and a one-trilayer SAS film (step iii, Scheme 2). The solid line shows the best fit using eq 1. The corresponding electron density profiles obtained from this fit are presented in Figure 7B. Similar reflectivity patterns and electron density profiles were obtained for all samples (for example, see the reflectivity data for the five-trilayer sample in the inset of Figure 8). The data show pronounced "Kiessig

(32) (a) Nijmeijer, A.; Kruidhof, H.; Bredesen, R.; Verweij, H. *J. Am. Ceram. Soc.* **2001**, *84*, 136. (b) Krongelb, S. *Electrochem. Technol.* **1968**, *6*, 251.
(33) (a) Tidswell, I. M.; Ocko, B. M.; Pershan, P. S. *Phys. Rev. B* **1990**, *41*, 1111. (b) Pomerantz, M.; Segmuler, A.; Netzer, L, Sagiv, J. *Thin Solid Films* **1985**, *132*, 153. (c) Tidswell, I. M.; Rabedeau, T. A.; Pershan, P. S.; Kosowsky, S. D.; Folkers, G. P.; Whitesides, G. M. *J. Chem. Phys.* **1991**, *95*, 2854.

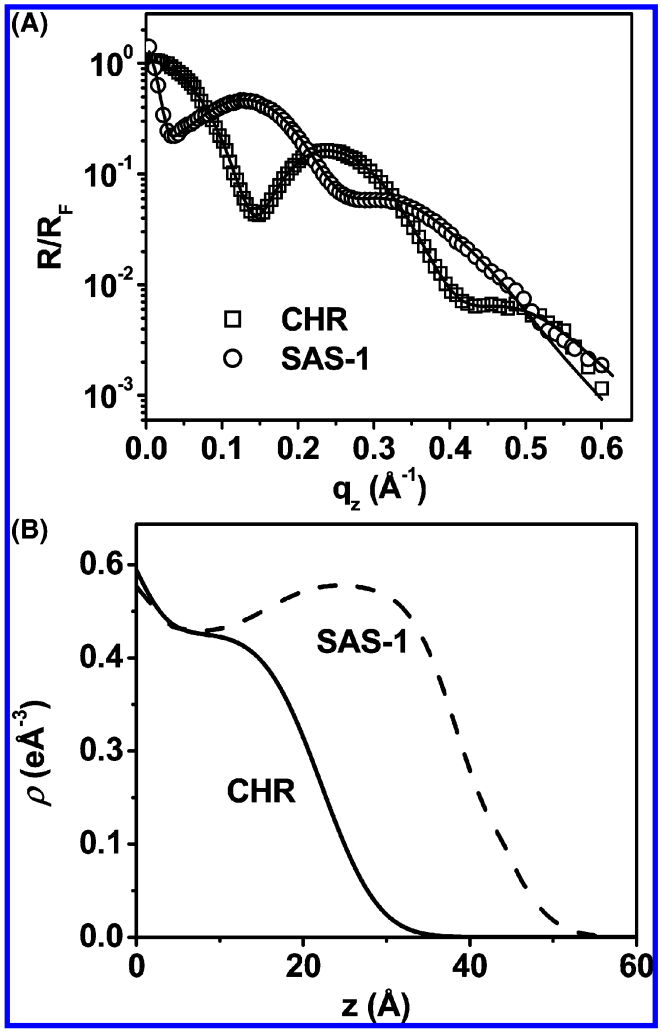

Figure 7. X-ray reflectivity data for films containing chromophore monolayer (**CHR**, step ii, Scheme 2) and one trilayer sample (**SAS-1**, step iii, Scheme 2). The structural model used for fitting the X-ray reflectivity data consists of a semi-infinite silicon substrate, a silicon oxide layer, a coupling layer, a self-assembled chromophore layer, and a capping layer. (A) X-ray reflectivity data normalized to the Fresnel reflectivity R_F for **CHR** (□) and **SAS-1** (○). The solid line is the best fit to the data. (B) The corresponding electron density profiles for **CHR** (solid line) and **SAS-1** (dashed line) obtained from this fit.

fringe" minima, corresponding to destructive interference of reflections from the top and bottom of the film, and indicate a narrow distribution of layer thicknesses.[8b,9,10,34] The total thickness of the film, T, can be found simply by using path length differences: $T = 2\pi/\Delta q_z$, where Δq_z is the spacing between the minima. The film thickness increases linearly as a function of the number of trilayers (Figure 8), underscoring the high structural regularity and efficiency of this approach. From the slope of the XRR data, an average interlayer spacing of 40.6 Å can be deduced. This thickness is found to be in a reasonable range using Spartan-level molecular modeling. The densities of electrons per unit of substrate area, ρ_{exp}, for the films were calculated using the electron density profiles according to $\rho_{exp} = \int \rho(z)\, dz$, where the integration is taken over the entire film. The "molecular footprint" can then be calculated from N_e/ρ_{exp}, where N_e is the total amount of electrons in a single

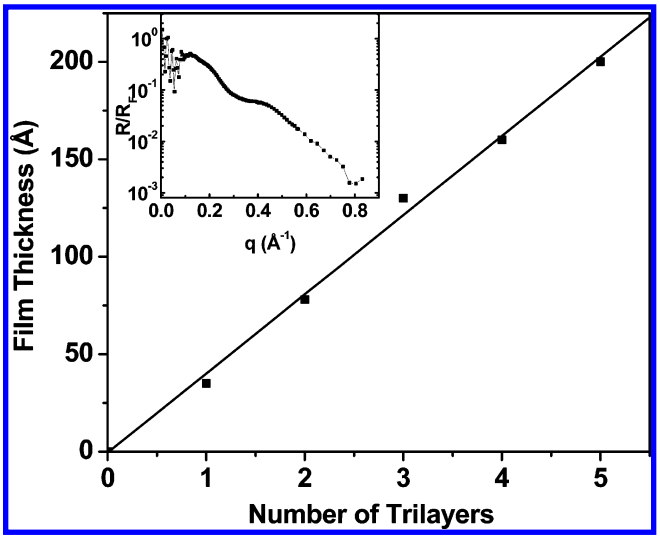

Figure 8. Specular X-ray reflectivity (XRR)-derived film thickness (Å) for X chromophore self-assembled films as a function of the number of trilayers. Inset: XRR data for a five-trilayer sample.

chromophore. The chromophore monolayer (step ii, Scheme 2) has an electron density of ~0.48 eÅ^{-3}, thickness of 22.2 Å, film roughness of 5.4 Å, and a molecular footprint of ~80 Å^2. This XRR-derived surface roughness is comparable to those of azobenzene and heterocycle-based monolayers (3.3−6.4 Å)[9,10a,b] and to that of highly ordered, self-assembled octadecyltrichlorosilane films on single-crystal silicon.[35] From the molecular footprint of a chromophore monolayer, the chromophore density (N_s) can be calculated and is found to be ~1.3×10^{14} molecules/cm^2. The one-trilayer SAS film (step iii, Scheme 2) has a thickness of ~35.0 Å, film roughness of 5.7 Å, and a footprint of ~80 Å^2. The capping layer structure is characterized by the comparison of electron density profiles of chromophore monolayer and one-trilayer SAS films (Figure 7B) to be a densely packed polysiloxane network with a thickness of ~15.3 Å, comprising roughly ~6 (−Si−O) repeat units.

Polarized angle-dependent second harmonic generation (SHG) measurements on the X chromophore self-assembled thin films were carried out at $\lambda_o = 1064$ nm in the transmission mode. The characteristic SHG interference pattern from a glass substrate coated on both sides is shown in Figure 9 inset, demonstrating that essentially identical film quality and uniformity are achieved on both sides of the substrates.[7−10] The presence of near-zero intensity minima indicates that the quality and uniformity of the deposited films on each side of the substrate is nearly identical. Moreover, the quadratic dependence of the 532 nm output intensity ($I^{2\omega}$) on film thickness (Figure 9) further demonstrates polar microstructure preservation as layer-by-layer assembly progresses.[7−10] By calibrating the angle-dependent SHG data against quartz, a large second-order macroscopic NLO response $\chi^{(2)}_{333} \sim 232$ pm/V at 1064 nm is obtained for X chromophore self-assembled films. Note that this value was obtained under nominally nonresonant conditions since the X chromophore has no significant optical absorption near 532 nm ($I^{2\omega}$).

(34) (a) Richter, A. G.; Durbin, M. K.; Yu, C.-J.; Dutta, P. *Langmuir* **1998**, *14*, 5980. (b) Malik, A.; Durbin, M. K.; Richter, A. G.; Huang, K. G.; Dutta, P. *Phys. Rev. B* **1995**, *52*, 11654.

(35) (a) Bierbaum, K.; Kinzler, M.; Wöll, Ch.; Grunze, M.; Hähner, G.; Heid, S.; Effenberger, F. *Langmuir* **1995**, *11*, 512. (b) Ohtake, T.; Mino, N.; Ogana, K. *Langmuir* **1992**, *8*, 2081. (c) Tidswell, I. M.; Ocko, B. M.; Pershan, P. S.; Wasserman, S. R.; Whitesides, G. M.; Axe, J. D. *Phys. Rev. B* **1990**, *41*, 1111.

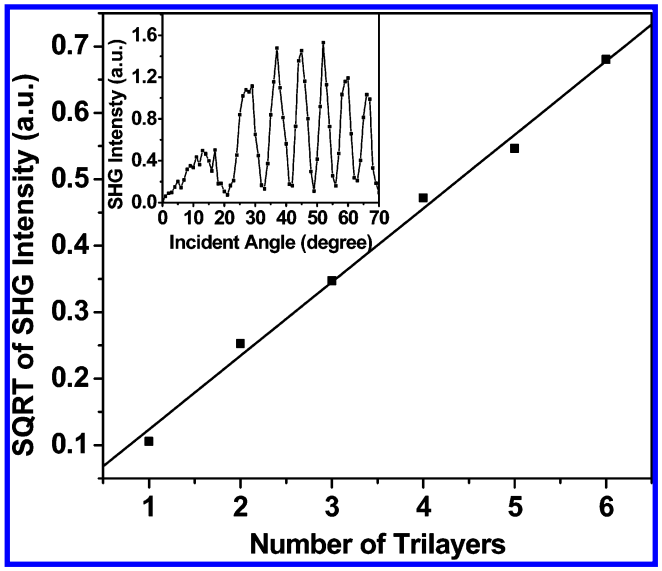

Figure 9. Square root of X chromophore self-assembled film 532 nm SHG response ($I^{2\omega}$, arbitrary units) as a function of the number of trilayers. Inset: SHG response as a function of fundamental beam incident angle from a float glass slide having a film on either side.

Contact mode AFM measurements were performed on each of five SAS samples, from one to five trilayers. This study reveals an increased grain texture and an RMS surface roughness going from 5.6 to 12.4 Å, respectively, for 1 × 1 μm^2 scan areas (Figure 10). Grain formation is a common phenomenon in layer-by-layer assemblies.[9,10] The RMS surface roughnesses compare favorably with those derived by XRR.

Discussion

Synthetic Strategies. To asymmetrically introduce all (*E*)-arylvinylene D/A functionalities, an orthogonal approach is applied using a sequence of the Wittig−Horner olefination and Heck coupling reactions. It begins with the separate synthesis of the aromatic "arms" terminated by aldehyde and vinyl functionalities and the construction of a "core" containing double *o*-phosphonate-activated methylene groups and double *o*-bromo groups. The Wittig−Horner reactions between the phosphonate core **2** and TBDMS-protected 4-[*N*,*N*-bis(2-hydroxyethyl)amino]-benzaldehyde **3** afford the desired two all-(*E*)-phenylenevinyl arms in 54% yield. The remarkable *E* stereoselectivity achieved with aryl-stabilized phosphonates has been widely demonstrated in the literature and is commonly employed to prepare (*E*)-stilbenes.[36] In contrast, conventional Wittig olefination employing double *o*-triphenylphosphonium ylides, in the present synthesis, results in a mixture of *Z*/*E*-isomers and in significantly lower yield. This is clearly a result of the weak stereoselectivity of triphenylphosphonium ylides bearing mildly conjugating phenyl substituents,[36] whereas the Heck reaction is known to be highly *E* stereoselective.[37] The subsequent double Heck coupling reaction results in the other two all-(*E*)-pyridine-vinyl arms. The observed coupling constant ^3J values for the vinyl protons in the **BPBAB** and **X-CHR** ^{1}H NMR spectra are all ∼16.0 Hz, consistent with an all-*E* configuration.

Optical Properties. The **X-CHR** chromophore exhibits a remarkably blue-shifted optical absorption maximum both in CH_2Cl_2 solution (357 nm) and in the self-assembled superlattices

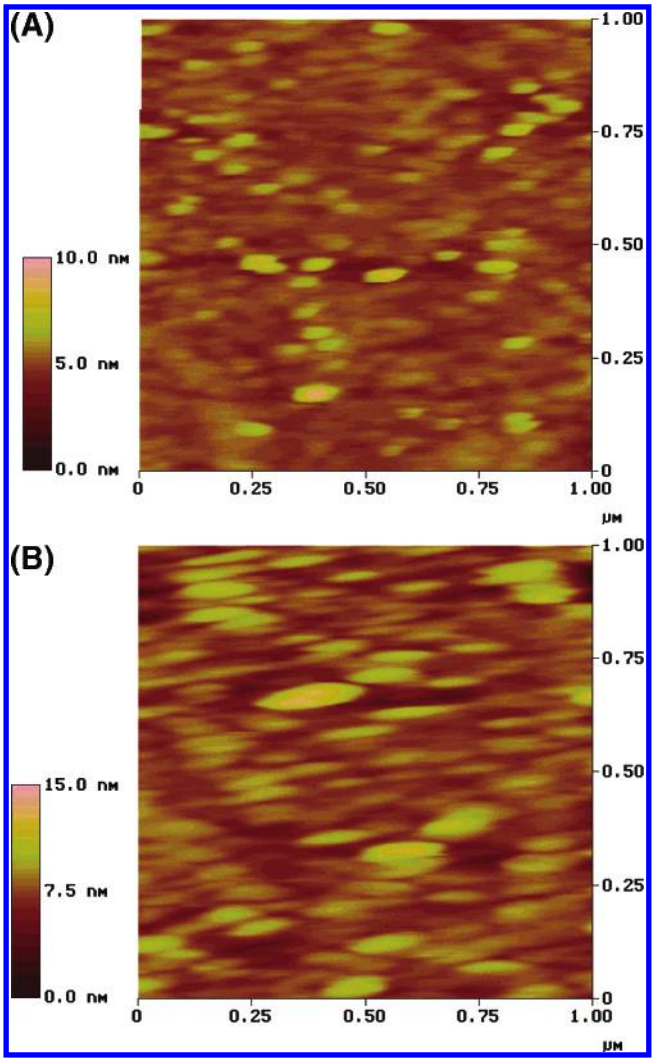

Figure 10. AFM images at 1 × 1 μm scan areas of X chromophore self-assembled films composed of one (A) and five (B) trilayers.

(325 nm), consistent with the AM1/ZINDO computed HOMO−LUMO CT excitation of λ_{max} = 369 nm for this chromophore.[18] The blue-shifted X chromophore HOMO−LUMO CT excitation can be understood to first order in terms of the excitonic coupling of transition dipoles. According to molecular exciton theory,[38] the angle between the transition dipoles and their interconnected axis, θ, is a key parameter defining the direction and magnitude of the band shift (see Figure 11A). The excitonic coupling of transition dipoles leads to a first excited state composed of a pair of excitonic states (Figure 11A). In the case of $\theta > 54.7°$, excitation to the upper excitonic state is optically allowed, and optical transitions from the ground state populate the upper excitonic state, resulting in the spectral blue-shift. When $\theta < 54.7°$, excitation to the lower excitonic state is optically allowed, and optical transitions from the ground state populate the lower excitonic state, resulting in the spectral red-shift. In the X chromophore, *intramolecular* coupling of transition dipoles in 2D is therefore sufficiently strong as to afford a dramatically blue-shifted optical maximum.

(36) Maryanoff, B. E.; Reitz, A. B. *Chem. Rev.* **1989**, *89*, 863.
(37) (a) Beletskaya, I. P.; Cheprakov, A. V. *Chem. Rev.* **2000**, *100*, 3009. (b) Cabri, W.; Candiani, I. *Acc. Chem. Res.* **1995**, *28*, 2. (c) de Meijere, A.; Meyer, F. E. *Angew. Chem., Int. Ed. Engl.* **1994**, *33*, 2379.
(38) Kasha, M.; Rawls, H. R.; Ashraf El-Bayoumi, M. *Pure Appl. Chem.* **1965**, *11*, 371.

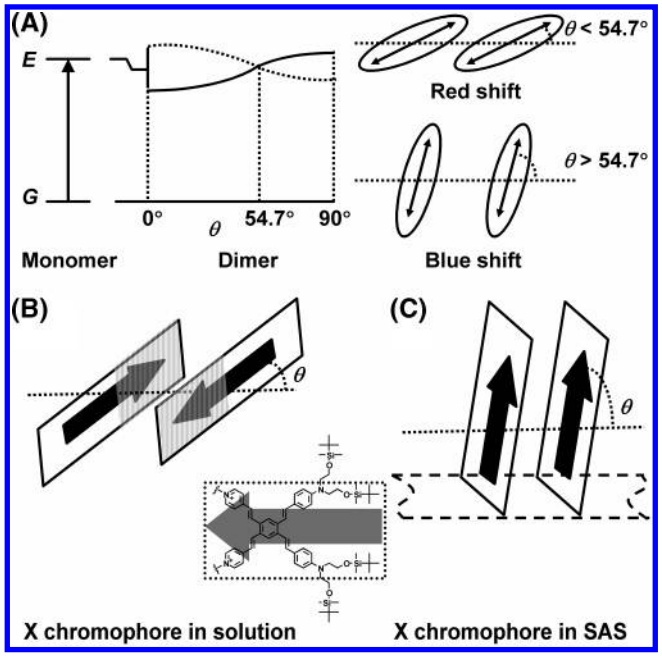

Figure 11. (A) Exciton band energy diagram for a molecular dimer with coplanar transition dipoles inclined with respect to the interconnected axis by the angle θ.[38] (B) Schematic description of presumed aggregation of **X-CHR** in solution with $\theta < 54.7°$, resulting in a blue-shift. Arrows show the directions of dipole moments. (C) Schematic depiction of the organization of the X chromophore in self-assembled superlattices with $\theta > 54.7°$, resulting in a blue-shift. Arrows show the directions of dipole moments.

In X chromophore solutions, concentration-dependent ^{1}H NMR spectroscopy (Figure 4) reveals that the chromophore molecules are aggregated primarily between the pyridine vinyl arm portions through $\pi-\pi$ interactions, while the other two phenylenevinyl arm portions cannot undergo close stacking due to the bulky TBDMS protecting groups, thus resulting in an antiparallel aggregate with two considerably slipped chromophore molecules (e.g., Figure 11B). The chromophores presumably aggregate in a "head-to-head"-like manner ($\theta < 54.7°$), a type of *J*-aggregation, consistent with the **X-CHR** UV−vis spectra in CH_2Cl_2 solution, where a bathochromically shifted aggregation band is observed (Figure 3).

The additional blue-shifting of the film λ_{max} versus that in solution (Figures 3 and 6) is consistent with *intermolecular* dipole−dipole coupling within the closely packed chromophore layers, where strong $\pi-\pi$ interactions are likely.[39] The AM1 semiempirical quantum mechanical energy-minimized structure of a "bidentate" quaternized X chromophore unit, with two covalently anchored siloxane functionalities fixed on an imaginary plane, yields a thickness of 24.5 Å. Comparing this thickness with the XRR-derived chromophore monolayer thickness of 22.2 Å argues that the chromophores are more or less perpendicular to the surface and θ reaches a value of ~65° (see Figure 11C). In this case, a blue-shift of the electronic transition is expected. In addition to θ, intermolecular distances and aggregation number will influence the spectral evolution. In particular, the magnitude of the band shift is also an index of the structural order within the monolayer. Such spectral shifts are well-known for azobenzene and other dyes in closely packed self-assembled monolayers and LB films.[40]

X Chromophore NLO/EO Properties. The HRS measurements provide the principal molecular tensor element $\beta_{zzz} = (1840 \pm 80) \times 10^{-30}$ esu. Since the second harmonic wavelength (400 nm) is close to the wavelength of the electronic resonance in **X-CHR** (340 nm in methanol), the resonance enhancement effect on the dynamic β_{zzz} value obtained at 800 nm must be taken into account. Applying the simple two-level model,[41] the static, intrinsic first hyperpolarizability β_0 can be estimated from the experimental HRS β_λ according to eq 2:

$$\beta_0 = \beta_\lambda(1 - (2\lambda_{max}/\lambda)^2)(1 - (\lambda_{max}/\lambda)^2) \quad (2)$$

Here λ is the HRS fundamental wavelength, and λ_{max} is the maximum absorption wavelength. We derive a resonance enhancement factor of 4.40. β_0 can be then estimated to be $(420 \pm 17) \times 10^{-30}$ esu, in excellent agreement with the AM1/ZINDO computation-derived $\beta_{\omega=0}$ of 407×10^{-30} esu.[18]

The X chromophore self-assembled thin films exhibit a second-order NLO macroscopic response $\chi^{(2)}_{333} \sim 232$ pm/V at 1064 nm, larger than that of related azobenzene-based self-assembled superlattices ($\chi^{(2)}_{333} \sim 180$ pm/V at 1064 nm).[9c] Moreover, these X-chromophore-based films are completely transparent at the fundamental laser wavelength and at the 532 nm SHG output wavelength (2ω) (Figure 6). Therefore, resonant enhancement due to overlap between the film CT absorption ($\lambda_{max} = 325$ nm) and the second harmonic wave should be relatively small, while it is known that such resonant effects can enhance experimental azobenzene-based SAS film ($\lambda_{max} = 575$ nm) nonlinearities by as much as 1 order of magnitude.[42] The EO coefficient r_{33} can be related to $\chi^{(2)}_{333}$ according to eq 3,[43] reasonably assuming a two-level dispersion model and neglecting dispersion of the local field factors.

$$r_{33} = \frac{2}{n^4}\frac{(3\omega_0^2 - \omega^2)(\omega_0^2 - \omega'^2)(\omega_0^2 - 4\omega'^2)}{3\omega_0^2(\omega_0^2 - \omega^2)^2}\chi^{(2)}_{333} \quad (3)$$

Here ω and ω' are EO and SHG fundamental frequencies, respectively (i.e., 1310 and 1064 nm, respectively); ω_0 is the first resonance frequency (corresponding to λ_{max}), and n is the refractive index. Reasonably assuming an index of refraction of 1.6 for self-assembled organic films of this type,[10b,c] r_{33} at a 1310 nm EO working fundamental is estimated to be ~45 pm/V for X-chromophore-derived SAS films versus ~9.4 pm/V for the azobenzene-based SAS film. It can be seen that the electro-optic response of X-chromophore-based film is comparable to those of other high-efficiency organic-based films[44] and inorganic materials, such as $LiNbO_3$ ($r_{33} = 31$ pm/V at 1310 nm).[2c,d]

Structural Characteristics of Self-Assembled X Chromophore Superlattices. Our previous studies established that the present layer-by-layer self-assembly procedure affords microstructurally regular polar multilayer superlattices without loss of acentricity (randomization of chromophore orientation)

(39) (a) Gunatatne, T.; Kennedy, V. O.; Kenney, M. E.; Rodgers, M. A. J. *J. Phys. Chem. A* **2004**, *108*, 2576. (b) Engelking, J.; Wittemann, M.; Rehahn, M.; Menzel, H. *Langmuir* **2000**, *16*, 3407.
(40) (a) Nieuwkerk, A. C.; Marcelis, A. T. M.; Sudhöter, E. J. R. *Langmuir* **1997**, *13*, 3325. (b) Everaars, M. D.; Marcelis, A. T. M.; Sudhöter, E. J. R. *Langmuir* **1996**, *12*, 3964. (c) Shimomura, M.; Aiba, S.; Tagima, N.; Inoue, N.; Okuyama, K. *Langmuir* **1995**, *11*, 969.
(41) Qudar, J. L.; Chemla, D. S. *J. Chem. Phys.* **1977**, *66*, 2664.
(42) (a) Lundquist, P. M.; Yitzchaik, S.; Zhang, T.; Kanis, D. R.; Ratner, M. R.; Marks, T. J.; Wong, G. K. *Appl. Phys. Lett.* **1994**, *64*, 2194. (b) Wang, L.; Yang, Y.; Marks, T. J.; Liu, Z.; Ho, S.-T. *Appl. Phys. Lett.* **2005**, *87*, 161107/1.
(43) Singer, K. D.; Kuzyk, M. G.; Sohn, J. E. *J. Opt. Soc. Am.* **1987**, *4*, 968.
(44) (a) Penner, T. L.; Motschmann, H. R.; Armstrong, N. J.; Ezenyilimba, M. C.; Williams, D. J. *Nature* **1994**, *367*, 49. (b) Robinson, B. H.; et al. *Chem. Phys.* **1999**, *245*, 35.

and diminution of SHG efficiency,[9,10] and that the efficient "topotactic" approach[10c−f] dramatically increases the rate of the related azobenzene chromophore deposition and results in self-assembled chromophoric films with greatly enhanced structural regularity and second-order optical nonlinearity. In the present study, it can be further seen that this topotactic approach successfully provides 2D X chromophore deposition, where double quaternization is crucial. Incomplete, single quaternization, which would result in alteration of the chromophore optical properties, disorder of chromophore alignment, and diminution of chromophore NLO response, is apparently minimal. The XRR-derived molecular footprint of the X chromophore monolayer is found to be ∼80 Å^2, approximately twice that of the self-assembled 4-ICH$_2$C$_6$H$_4$SiCl$_2$I coupling layer (∼40 Å^2, step i, Scheme 2).[10a,c] It therefore appears that each X chromophore is favorably anchored at two adjacent surface benzyl iodide functionalities of the coupling layer (step ii, Scheme 2), and an almost complete surface quaternization/coverage is achieved. This surface chromophoric coverage is slightly larger than those of related 1D azobenzene and heterocycle-based chromophore SA films (footprint ∼ 47−57 Å^2) deposited on the similar coupling layer surface, where the degree of surface quaternization of chromophore precursor is found to be 80−90% of the available surface benzyl halide groups.[10a,c] This result suggests that the double pyridylvinyl functionalities in X chromophore, a bidentate-like form, may facilitate the self-limiting chemisorption of the chromophore units via a type of "chelate effect", providing a greater packing density than those of related 1D chromophores. It is well-known in coordination chemistry that metal−ligand complexes possessing chelating ligands exhibit enhanced stabilities versus nonchelating analogues.[45] This entropy-driven chelate effect is also found to provide well-packed and highly oriented self-assembled monolayers on gold generated from bidentate thiols[46] and on ITO surfaces formed from multi-chlorosilane-tethered molecules.[47] In addition, likely $\pi-\pi$ interactions between X chromophore π system planes (as seen in the blue-shifted λ_{max} of the X chromophore SA film, vide supra) may also facilitate greater structural regularity/packing density. Addition of subsequent layers results in an equal molecular footprint of ∼80 Å^2 (step iii, Scheme 2), indicating that the footprint remains constant upon multilayer formation.

The uniform growth of the self-assembled multilayers is indicated by the linear dependence of the X chromophore longitudinal HOMO−LUMO charge-transfer absorbance at 325 nm on the number of assembled trilayers (Figure 6) as well as by the linear dependence of X-ray reflectivity-derived multilayer thicknesses on the number of assembled trilayers (Figure 8). Multilayer structural uniformity is further evidenced in the AFM images that show that the present multilayer films have very smooth surface morphologies (Figure 10). Finally, for a microstructurally regular polar multilayer, with minimal self-absorption, the SHG intensity ($I^{2\omega}$) is expected to scale quadratically with the number of chromophore deposition cycles because the incident light wavelength (1.06 μm) is large compared to the SA film thickness.[9,10] Indeed, the observed linear dependence of $(I^{2\omega})^{1/2}$ on the number of trilayers demonstrates (Figure 9) that approximately equal densities of uniformly polar-oriented chromophores are deposited in each assembled trilayer while maintaining good structural regularity.

Conclusions

We have shown that a novel type of X-shaped 2D EO chromophore with extended conjugation displays a markedly blue-shifted optical maximum (357 nm in CH_2Cl_2) while maintaining a very large first hyperpolarizability. HRS measurements on the new chromophore at an 800 nm fundamental wavelength provide a β value of 1840×10^{-30} esu. Both the experimental linear and nonlinear optical response properties exhibit good agreement with computational predictions. The new chromophore can be successfully integrated into structurally regular and acentric self-assembled multilayer films via a layer-by-layer chemisorptive siloxane-based approach. The chromophoric film exhibits a dramatically blue-shifted optical maximum (325 nm) while maintaining a large EO response ($\chi^{(2)}_{333} \sim 232$ pm/V at 1064 nm; $r_{33} \sim 45$ pm/V at 1310 nm). This work demonstrates an attractive approach to developing EO materials offering improved nonlinearity−transparency trade-off characteristics. Further studies will focus on optimizing β response and optical properties, as well as on an in-depth understanding of this special nonlinearity−transparency relationship by a combination of molecular modeling and modification.

Acknowledgment. We thank DARPA/ONR (SP01P7001R-A1/N00014-00-C) and the NSF-Europe program (DMR-0353831) for support of this research. We thank the Northwestern University MRSEC for support of characterization facilities (DMR 0076077). X-ray reflectivity measurements were performed at Beam Line X23B of the National Synchrotron Light Source, which is supported by the U.S. Department of Energy. We thank Dr. S. Keinan and Prof. M. Ratner for computational collaboration, and Drs. P. Zhu and A. Facchetti for helpful discussions.

Supporting Information Available: Complete ref 44b. This material is available free of charge via the Internet at http://pubs.acs.org.

JA060185V

(45) Purcell, K. F.; Kotz, J. C. *Inorganic Chemistry*; W. B. Saunders: Philadelphia, 1977.
(46) (a) Grag, N.; Lee, T. R. *Langmuir* **1998**, *14*, 3815. (b) Shon, Y.-S.; Lee, T. R. *Langmuir* **1999**, *15*, 1136. (c) Park, J.-S.; Vo, A. N.; Barriet, D.; Shon, Y.-S.; Lee, T. R. *Langmuir* **2005**, *21*, 2902.
(47) Huang, Q.; Evmenenko, G. A.; Dutta, P.; Lee, P.; Armstrong, N. L.; Marks, T. J. *J. Am. Chem. Soc.* **2005**, *127*, 10227.